CrystEngComm

ROYAL SOCIETY OF CHEMISTRY

PAPER

View Article Online
View Journal | View Issue

Cite this: *CrystEngComm*, 2023, **25**, 1479

Synthesis, structure and magnetic properties of two bis(oxalato)cuprate(II) salts with pyridinium type counter ions†

Cyrielle L. F. Dazem,[a] A. Ken Inge,[b] Dominique Luneau,[c] Lars Öhrström *[d] and Justin Nenwa*[a]

Mono- and a di-protonated pyridine type cations have been used for the synthesis of two bis(oxalato) cuprate(II) salts, namely, $(C_5H_7N_2O)_2[Cu(C_2O_4)_2]$ ($C_5H_7N_2O$ = 2-amino-3-hydroxypyridinium) **1** and $C_{13}H_{16}N_2[Cu(C_2O_4)_2]$ ($C_{13}H_{16}N_2$ = 4,4′-trimethylenedipyridinium) **2**. In the crystal structures, $C_2O_4^{2-}$ adopts different coordination modes: the common bidentate chelating oxalate in **1** and the relatively scarce μ-oxalato-$\kappa^3O^1,O^2:O^{1'}$ in **2**. X-ray diffraction also revealed that $[Cu(C_2O_4)_2]^{2-}$ anions do not polymerize in **1** (a phenomenon hardly observed in such salts), while in **2**, the polymerization of $[Cu(C_2O_4)_2]^{2-}$ units occurs *via* the Cu–O_{axial} contact forming a zigzag Cu(II) chain. In complex **1**, the emerging building blocks are linked into 2D supramolecular layers *via* N–H···O and O–H···O hydrogen bonds and weaker C–H···O interaction to form a 3D net. In contrast to **2**, the emerging building blocks are linked into 1D chains *via* N–H···O hydrogen bonds, which further extend to form a 3D supramolecular framework through Cu–O_{axial} and other C–H···O interactions. The structural diversities show that iminium counterions play key roles in the construction of various architectures. Thermal analyses showed no weight loss for either system in the temperature range of 20–180 °C, which indicates that none of these complexes possess solvation water molecules. Magnetic studies indicate the presence of antiferromagnetic coupling between the spin centres in **1** and **2**.

Received 7th November 2022,
Accepted 16th December 2022

DOI: 10.1039/d2ce01513g

rsc.li/crystengcomm

1. Introduction

Oxalates are ubiquitous. They are found in numerous plants but may also form less pleasant kidney and bladder stones in humans. The latter comprise calcium oxalates, and other oxalate complexes with metal ions are used, for example, in artistic chemical photography processes and the anticancer drug oxaliplatin (elotaxin).[1]

However, oxalates are abundant also in today's research, and we have lately reported on oxalate networks and on naturally occurring metal–organic frameworks (MOFs).[2] Recently, metal oxalates have also been featured in the production of the medical radioisotope ^{89}Zr,[3] and freestanding oxalate ions were reported as crystalline molecular rotors in salts with $[M(en)_3]^{2+}$ serving as a molecular stator.[4] Perhaps the more obvious work is on oxalate MOFs[5] and copper oxalates for magnetic devices for chemical sensing.[6]

Over the past years, great efforts have been devoted to the self-assembly of organic–inorganic molecules in the solid state for different reasons: i) it offers extraordinary structural versatility and allows the formation of fascinating structures[7,8] – in fact the framework flexibility has been highlighted as an advantage for high-performance molecular recognition, separation and sensing application,[9] ii) it extends the range of designing functional solid materials from neutral or ionic molecular-based building blocks properties,[10,11] and iii) it allows the search of new structural topologies and connectivities in the solid state.[2]

Research activities mostly involve organic cations with metal complex anions as an inorganic entity, organic–inorganic salts. The versatile coordination modes and the ability to transmit the electronic effects between magnetic centres separated by more than 5 Å[12,13] and to form interesting hydrogen-bonded solid state networks could

[a] *Inorganic Chemistry Department, Faculty of Science, University of Yaoundé I, PO. Box 812, Yaoundé, Cameroon. E-mail: cyrielle_leyla@yahoo.fr, jnenwa@yahoo.fr*
[b] *Department of Materials and Environmental Chemistry, Stockholm University, Stockholm, SE-106 91 Sweden*
[c] *Laboratoire des Multimatériaux et Interfaces (UMR 5615), Université Claude Bernard de Lyon 1, Campus de la Doua, 69622 Villeurbanne, France. E-mail: dominique.luneau@univ-lyon1.fr*
[d] *Chemistry and Biochemistry, Dept. of Chemistry and Chemical Engineering, Chalmers University of Technology, SE-41296 Göteborg, Sweden. E-mail: ohrstrom@chalmers.se*

† Electronic supplementary information (ESI) available. CCDC 1848472, 1848473, 2217520, and 2217521. For ESI and crystallographic data in CIF or other electronic format see DOI: https://doi.org/10.1039/d2ce01513g

justify the special attention paid towards the investigation of salts based on the oxalate(2-) ligand.[14]

Among the various anionic transition metal oxalates, the copper(II) ones have been considered attractive building blocks for the construction of organic–inorganic salts in recent years.[15] One of the most interesting organic cation–copper oxalate combinations is that of pyridinium derivatives and anionic bis(oxalato)cuprate(II) complexes. Compared to many Cu(II) oxalate organic–inorganic salts based on ammonium-based counterions, pyridinium ones are still less explored. Moreover, with the structural variability observed in the reported pyridinium salts, the understanding of their basic properties is still ongoing. Therefore, more work is required to understand the factors that influence the resulting crystal structure. With regards to the wide range of pyridinium-based cations, there is still a broad chemical space for synthesizing new organic–inorganic compounds with unusual structures and unknown properties.

For five years now, our research group has been investigating pyridinium-type counterion salts with bis(oxalato)cuprate(II) anions, with a view not only to producing new functional materials but also to unraveling the subtle structural features that characterize these solids. Accordingly, we previously successfully contributed to these endeavours with three novel pyridinium derivatives of Cu(II) oxalate salts, namely, bis(3-aminopyridinium) bis(oxalato)cuprate(II) dihydrate, bis(2-amino-4,6-dimethylpyridinium) bis(oxalato)cuprate(II)penta-hydrate,[16] and bis(2-amino-pyridinium) bis(oxalato)cuprate(II) trihydrate.[17] Recently ternary co-crystal salts, namely, bis(3-aminopyridinium) bis(oxalato)cuprate(II) dioxalic acid and bis(4-dimethylaminopyridinium) bis(oxalato) diaquacuprate(II) oxalic acid, were also prepared and structurally characterised.[18]

Encouraged by these results we continued with this type of salt and investigated the self-assembly of bis(oxalato)cuprate(II) anionic units with pyridinium derivatives containing amino(–NH_2) and hydroxyl (–OH) functional groups and an alkyl $(–CH_2–)_n$ group between two pyridinium ions (Fig. 1). We report here the synthetic and structural characterization of $(C_5H_7N_2O)_2[Cu(C_2O_4)_2]$ **1** and $C_{13}H_{16}N_2[Cu(C_2O_4)_2]$ **2**, as well as their spectroscopic analysis and magnetic properties ($C_5H_7N_2O$ = 2-amino-3-hydroxypyridinium and $C_{13}H_{16}N_2$ = 4,4′-trimethylenedipyridyl).

2. Experimental

2.1 Materials and methods

2.1.1 Physical methods. Elemental analysis of C, H and N was performed on a Perkin-Elmer 2400 CHN elemental analyzer. IR spectra were recorded in the range 4000–400 cm^{-1} on a Bruker Equinox 55 spectrophotometer with pressed KBr pellets. Electronic absorption spectra were collected on a Perkin-Elmer Lambda 900 spectrophotometer from 350 to 900 nm in water solution. TGA-DSC analyses were performed using a Delta Series TA-SDTQ 600 in a flowing air atmosphere with a heating rate of 10 °C min^{-1} from 25 to 800 °C using alumina crucibles. Powder X-ray diffraction (PXRD) measurements were executed on a Bruker D8 ADVANCE X-ray diffractometer with Cu Kα radiation at room temperature and also at 100 K for **1** with a Rigaku Synergy-R X-ray diffractometer. The surface morphology of both samples was investigated by scanning electron microscopy (SEM) using a JSF-7500F, and the elemental composition was determined by energy-dispersive X-ray spectroscopy (EDS) with a XSAM 800 spectrophotometer. The magnetic properties of the polycrystalline samples were measured using a Quantum Design MPMS-XL SQUID magnetometer at 0.1 T applied magnetic field in the temperature range 2–300 K. Magnetization isotherms were collected between 0–5 T. Diamagnetic corrections were made with Pascal's constants for all the constituent atoms, as well as the contributions of the sample holder.[19]

2.1.2 Synthesis. All reagents were purchased from commercially available suppliers and used as received without further purification. The precursor salt $(NH_4)_2[Cu(C_2O_4)_2]·2H_2O$ was prepared according to a literature protocol.[20]

*$(C_5H_7N_2O)_2[Cu(C_2O_4)_2]$ **1**.* A light brown solution containing oxalic acid dihydrate (126 mg, 1 mmol) and 2-amino-3-hydroxypyridine (220 mg, 2 mmol) in 20 mL of distilled water was stirred at 50 °C for 1 h. Subsequently, a blue aqueous solution of $(NH_4)_2[Cu(C_2O_4)_2]·2H_2O$ (311 mg, 1 mmol) was added into the aforementioned solution and stirred for an additional 30 min at a constant temperature of 50 °C. After the reaction was stopped and cooled, the resulting solution was filtered and stored at room temperature to produce dark green crystals of **1** after 14 days: yield *ca.* 96% [based on $(NH_4)_2[Cu(C_2O_4)_2]·2H_2O$]. X-ray powder diffraction was performed to confirm the purity of the sample. Anal. calcd (Found%) for $C_{14}H_{14}CuN_4O_{10}$ (Mr = 461.84): C, 36.38 (35.10); H, 3.03 (2.90); N, 12.13 (11.50). IR (KBr pellet, cm^{-1}): 3468(w), 3423(w), 3345(w), 3101(w), 1708(s), 1629(s), 1571(s), 1288(s), 1244(s), 795(s), 895(w), 586(w). UV-vis (H_2O solution, nm) 440; 713.

*$C_{13}H_{16}N_2[Cu(C_2O_4)_2]$ **2**.* A colourless solution containing oxalic acid dihydrate (126 mg, 1 mmol) and 4,4′-trimethylenedipyridine (200 mg, 1 mmol) in 20 mL of distilled water was stirred at 50 °C for 1 h. Subsequently, a blue aqueous solution of $(NH_4)_2[Cu(C_2O_4)_2]·2H_2O$ (311 mg, 1 mmol) was added into the aforementioned solution and stirred for an additional 30 min at a constant temperature of 50 °C. After the reaction was stopped and cooled, the resulting solution was filtered and stored at room temperature to produce dark blue crystals of **2** after 16 days: yield *ca.* 93% [based on $(NH_4)_2[Cu(C_2O_4)_2]·2H_2O$]. X-ray powder diffraction was performed to confirm the purity of

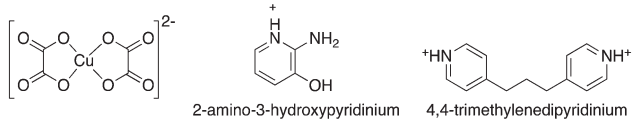

Fig. 1 Building blocks of $(C_5H_7N_2O)_2[Cu(C_2O_4)_2]$ (**1**) and $C_{13}H_{16}N_2[Cu(C_2O_4)_2]$ (**2**).

the sample. Anal. calcd (found%) for $C_{17}H_{16}CuN_2O_8$ (Mr = 439.87): C, 46.37 (45.90); H, 3.64 (3.50); N, 6.37 (6.20). IR (KBr pellet, cm^{-1}): 3436(m), 1666(m), 1671(s), 1641(s), 1498(m), 1413(s), 1286(s), 1203(m), 824(m), 542(w), 488(m). UV-vis (H_2O solution, nm): 721.

2.1.3 Crystallographic measurements. Single crystal X-ray diffraction data of **1** and **2** at 100 K were obtained by mounting suitable crystals on a nylon loop on an XtaLAB Synergy R, HyPix diffractometer. The crystals were kept at a steady T = 100.0(2) K during data collection. Their structures were solved with the ShelXT[21] structure solution program using the Intrinsic Phasing solution method and by using Olex2[22] as the graphical interface. The model was refined with version 2016/6 of ShelXL[21] using Least Squares minimisation. In addition 298 K and 293 K structures were obtained using a D8 Venture equipped with a PHOTON 100 CMOS detector (Mo Kα radiation, λ = 0.71073 Å). The structures were solved by direct methods and refined by full-matrix least squares techniques on F^2 using the SHELX-2014 software package.[21] All non-hydrogen atoms were refined with anisotropic displacement parameters. The positions of hydrogen atoms of organic cations were added in idealized geometrical positions. The graphics were drawn using CrystalMaker. The crystallographic data and details of the structure refinements are given in Table 1. CCDC 2217520 and CCDC 2217521 contain the crystallographic data for **1** and for **2**, respectively (1848473 and 1848472 for room temperature structures). These data can be obtained free of charge from the Cambridge Crystallographic Data Centre, *via* **https://www.ccdc.cam.ac.uk/conts/retrieving.html**.

Table 1 Crystallographic parameters for **1** and **2**

Compound	**1**	**2**
Empirical formula	$C_7H_7Cu_{0.5}N_2O_5$	$C_{17}H_{16}CuN_2O_8$
Formula weight	230.92	439.86
Temperature/K	99.9(4)	100.0(2)
Crystal system	Triclinic	Monoclinic
Space group	$P\bar{1}$	$P2_1/c$
a/Å	5.0894(3)	10.5484(2)
b/Å	7.1344(3)	22.2344(6)
c/Å	11.4050(4)	7.22640(18)
α/°	86.127(3)	90
β/°	77.266(4)	102.125(2)
γ/°	81.424(4)	90
Volume/Å^3	399.15(3)	1657.05(7)
Z	2	4
ρ_{calc}g/cm^3	1.921	1.763
μ/mm^{-1}	2.623	2.362
F (000)	235.0	900.0
Crystal size/mm^3	0.1 × 0.023 × 0.015	0.107 × 0.056 × 0.042
Radiation/Å	CuKα (λ = 1.54184)	CuKα (λ = 1.54184)
2Θ range for data collection/°	7.952 to 150.808	7.952 to 151.102
Index ranges	$-6 \le h \le 6$, $-8 \le k \le 8$, $-12 \le l \le 14$	$-9 \le h \le 12$, $-27 \le k \le 26$, $-9 \le l \le 9$
Reflections collected	6951	15792
Independent reflections	1571 [R_{int} = 0.0465, R_{sigma} = 0.0350]	3303 [R_{int} = 0.0340, R_{sigma} = 0.0233]
Data/restraints/parameters	1571/0/149	3303/0/261
Goodness-of-fit on F^2	1.092	1.069
Final R indexes [$I > = 2\sigma(I)$]	R_1 = 0.0359, wR_2 = 0.0975	R_1 = 0.0263, wR_2 = 0.0735
Final R indexes [all data]	R_1 = 0.0393, wR_2 = 0.0990	R_1 = 0.0290, wR_2 = 0.0747
CCDC deposition numbers	CCDC 2217520	CCDC 2217521

3. Results and discussion

3.1 Synthesis

Salts, namely, $(C_5H_7N_2O)_2[Cu(C_2O_4)_2]$ (**1**) and $C_{13}H_{16}N_2[Cu(C_2O_4)_2]$ (**2**) ($C_5H_7N_2O$ = 2-amino-3-hydroxypyridinium; $C_{13}H_{16}N_2$ = 4,4′-trimethylenedipyridinium) were obtained following two chemical processes similar to the one described by us for related compounds.[16] First the imine groups of the pyridine derivatives (DerPy) are protonated by oxalic acid, producing iminium cations $(DerPy\text{-}H)^+$. Second, an aqueous solution of $(NH_4)_2[Cu(C_2O_4)_2]\cdot 2H_2O$ was added, and the target compounds crystallised and were collected after around 2 weeks.

3.2 Single crystal X-ray structures

3.2.1 $(C_5H_7N_2O)_2[Cu(C_2O_4)_2]$ 1. X-ray diffraction structural analysis reveals that the asymmetric unit of **1** contains one-half Cu, one oxalate, and one ($C_5H_7N_2O$). In Fig. 2 we show the discrete metal–organic motif $[Cu(C_2O_4)_2]^{2-}$ and two 2-amino-3-hydroxypyridinium cations $(C_5H_7N_2O)^+$.

The Cu^{2+} ion exhibits a square-planar geometry with four O atoms from two chelating oxalato^{2-} ligands. However, there are also Cu–N interactions in the axial positions at 2.711(5) Å, and as the N1 geometry is distinctly non-planar with the N1 distance from the C7–H1A–H1B plane being 0.212 Å, we interpret this as a bonding interaction giving an overall octahedral configuration. We can thus also describe **1** as a neutral coordination compound. However, it needs to be noted that this Cu–N distance is a fair bit longer than the

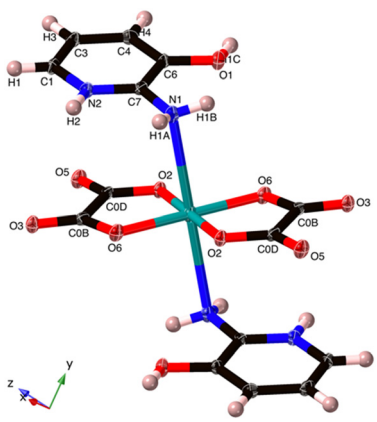

Fig. 2 The Cu coordination in $(C_5H_7N_2O)_2[Cu(C_2O_4)_2]$ **1**. The O5 hydroxyl group hydrogen bonds to O3 and the N1 amine. The axial Cu–N bond is 2.711(5) Å.

Cu–N peak of Jahn–Teller distorted compounds found in the CSD at 2.35–2.48 Å (Fig. S1†).

Cu1–O6 and Cu1–O2 are at two independent distances, namely, 1.936 (5) and 1.938 (5) Å, respectively. There are also two unique O6–Cu1–O2 bond angles of 84.80 (8) and 95.20 (8)°. These distances and angles are akin to those found in some reported Cu(II) oxalate salts featuring similar coordination motifs.[23,24]

The packing of **1** shows strong interlocking between complex anion and cationic sub-lattices through a multidirectional hydrogen bonding network. The organic cations, $(C_5H_7N_2O)^+$, link adjacent copper oxalate anions *via* hydrogen bonding interactions N2–H2···O2, N1–H1A···O6 and O1–H1C···O3 to form a 1D chain in the *x*-direction (Table 2).

These chains are further linked by the axial Cu–N bonds in the *z*-direction, and a pair of organic cations, $(C_5H_7N_2O)^+$, bridges two neighbouring $[Cu(C_2O_4)_2]^{2-}$ units *via* weaker C–H···O hydrogen bonding interactions between C atoms from $(C_5H_7N_2O)^+$ and O atoms from $[Cu(C_2O_4)_2]^{2-}$ (O3···H3 at 2.49 Å and O5···H1 at 2.43 Å; see Fig. 3), to generate a 3D supramolecular network.

3.2.2 $C_{13}H_{16}N_2[Cu(C_2O_4)_2]$ 2. The basic structure unit of **2** is shown in Fig. 4. Its structure consists of $[Cu(C_2O_4)_2]^{2-}$ anion counterbalanced by the dication 4,4′-trimethylenedipyridinium. The molecular difference to **1** is primarily the larger cation, $(C_{13}H_{16}N_2)^{2+}$ *vs.* $(C_5H_7N_2O)^+$. 4,4′-Trimethylenedi-pyridinium also has greater bulk and fewer hydrogen bonding possibilities.

The Cu(II) centre in **2** shows a square pyramidal geometry with four oxygen atoms (O1, O4, O5, and O8) from two oxalate(2-) ligands in the equatorial plane and one terminal oxygen atom (O7) from the neighbouring $[Cu(C_2O_4)_2]^{2-}$ unit in the apical position. The length of Cu–O_{eq} bonds (Cu1–O6 = 1.957(1), Cu1–O7 = 1.934(1), Cu1–O11 = 1.935(2) and Cu1–O8 = 1.943(1) Å) are in good agreement to those in related Cu(II) complexes of 2,6-bis(4′-pyridyl-1′-pyridiniumyl) pyrazine[25] and aminoguanidinium;[26] the length of the Cu–O_{axial} bond (Cu–O7 = 2.454(2) Å) is consistent with the ones in known aminoguanidinium[26] and potassium[27] salts and normal for a Jahn–Teller Cu–O bond. The bite angles of the bidentate oxalate were within the expected bond angles.[25]

An extended analysis of this compound permitted us to notice that it is a single O-bridged copper coordination polymer constructed from oxalate ligands adopting a rare μ-oxalato-κ^{3}O, ^{1}O^2:O$^{1\prime}$ coordination mode.[26,28] We also note, in contrast to **1**, that the stacking of the anionic $[Cu(C_2O_4)_2]^{2-}$ entities occurs through the weak interaction between the Cu(II) ion and terminal O12 atom, leading to a uniform zigzag Cu(II) chain that runs along the crystallographic *z*-axis, Cu···Cu = 5.348 Å (Fig. 4). Interestingly, in the 4-(pyridin-1-ium-4-yl)piperazin-1-ium compound the μ-oxalato-κ^{3}O^1,O^2:O$^{1\prime}$ coordination mode results in a different polymer chain, and the one –CH_2– unit shorter 4,4′-dimethylenedipyridinium salt contains discrete $[Cu(C_2O_4)_2]^{2-}$ units.[28] Moreover, the aminoguanidinum compound, the second example of the μ-oxalato-κ^{3}O^1,O^2:O$^{1\prime}$ mode, adopts a staircase-type polymer chain.[26]

We also note that $(H_2CBpy)[Cu(C_2O_4)_2]\cdot 2H_2O$[29] has been found as a single O-bridged copper coordination polymer constructed from oxalate ligands. However, here we have a μ-oxalato-κ^{3}O^1,O^2:O^1 polymer, which is more commonly observed in these systems.

The organic and inorganic parts, arranged in an alternating manner, whichever *x* or *y* direction is chosen, are linked *via* N26–H26···O5, and N14–H14···O13 hydrogen

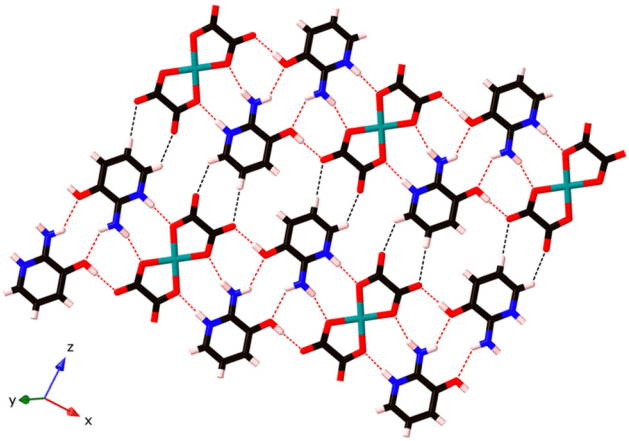

Fig. 3 The hydrogen bonded sheets in $(C_5H_7N_2O)_2[Cu(C_2O_4)_2]$ **1**. These are then connected to a 3D network by the weak axial Cu–N bonds; see Fig. 2. Strong hydrogen bonds in red and weak C–H hydrogen bonds in black.

Table 2 Strong hydrogen bond interactions in **1**

D	H	A	d(D–H)/Å	d(H–A)/Å	d(D–A)/Å	D–H–A/°
N2	H2	O2^1	0.96(3)	1.81(3)	2.764(2)	177(3)
O1	H1C	O3^2	0.85(4)	1.75(4)	2.602(2)	178(4)
N1	H1A	O6^3	0.91(3)	1.98(3)	2.862(3)	162(3)

^{1}3 − *x*, −*y*, 1 − *z*^{2}; 1 − *x*, 1 − *y*, 1 − *z*^{3}; 1 + *x*, +y, +z.

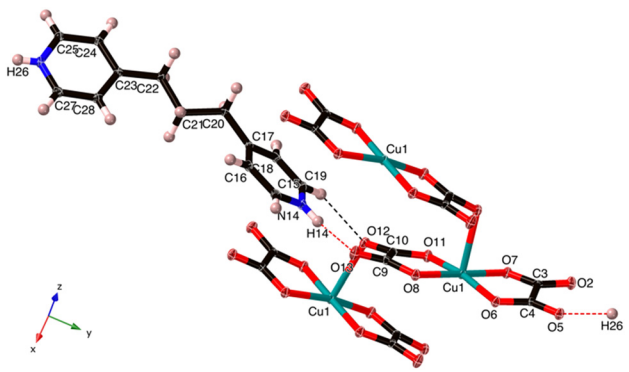

Fig. 4 The asymmetric unit of $C_{13}H_{16}N_2[Cu(C_2O_4)_2]$ (**2**) with one extra oxalate, one extra Cu and one additional N–H. The Cu–O7 is 2.538 Å, which is normal for an axial Jahn–Teller bond.

Table 3 Strong hydrogen bond interactions in **2**

D	H	A	d(D–H)/Å	d(H–A)/Å	d(D–A)/Å	D–H–A/°
N26	H26	O5[1]	0.77(2)	1.95(2)	2.7066(18)	165(2)
N14	H14	O13	0.82(2)	1.91(2)	2.6989(19)	161(2)

[1] $+x, -1+y, +z$.

bonds (Table 3 and Fig. 4) to form 1D cation-anion ribbons along the *y*-axis.

In addition, the 1D chains are extended through Jahn–Teller Cu–O_{axial} bonds, generating sheets parallel to the *yz* plane. Finally, two pairs of weak hydrogen bonds C15–H15···O5 at 2.22(3) Å and C18–H18···O2 at 2.26(3) Å connect the aforementioned sheets in the *xy*-plane to form a 3D supramolecular network (Fig. S7†).

Another way to look at the packing in the *xy*-plane is to consider the charges, and as shown in Fig. S8,† opposite charges form a kind of a chess board pattern.

3.3 IR spectra

The IR spectra of **1** and **2** are presented in Fig. S2.† They exhibit sharp absorption bands at around 1708–1670 cm^{-1} and 1288–1244 cm^{-1}, which can be attributed to the stretching modes of carboxyl COO^- groups.[30] Moreover, **1** has a weak absorption band at 3345 cm^{-1}, which can be ascribed to the stretching vibrations of the phenol hydroxyl group.[31]

3.4 UV-vis spectra in solution

The UV spectrum of **1** in water (Fig. 5 left) presents two broad and weak absorption bands at 440 and 713 nm (ε = 25.438 mol^{-1} L cm^{-1}), and that of **2** in water (Fig. 5 right) presents a broad and strong absorption band at 719 nm (ε = 48.245 mol^{-1} L cm^{-1}). In the case of **1**, the obtained bands are characteristic of Cu(II) metal centres with a square-planar geometry,[32,33] while those for **2** could suggest a square pyramidal geometry.[34,35] All these bands are due to the spin allowed intrametal (d–d) transition of the copper(II) center and are assigned to the envelope of the transitions from $^2B_{1g}$ (ground state to the excited $^2A_{1g}$ (d_{z^2})), $^2B_{2g}$ (d_{xy}) and ^2E_g (d_{xz}, d_{yz}) states.

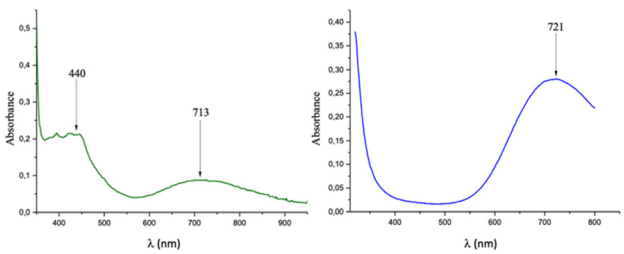

Fig. 5 UV-vis spectra of **1** (left) and **2** (right).

3.5 PXRD analysis and SEM

The powder X-ray diffraction (PXRD) pattern was used to verify the crystallinity and phase purity of **1** and **2**. The experimental and the simulated powder XRD patterns are presented in Fig. S4.† The experimental diffraction peak patterns of each complex are well defined, which demonstrates the crystallization of both complexes. We can also observe that the diffraction peaks of both experimental and simulated patterns match well in the key positions besides some intensity differences, which indicates a good phase purity for both compound and down to 100 K for **1**.

The surface morphologies of the as-prepared samples were investigated by scanning electron microscopy (SEM) and are shown in Fig. S9,† also indicating phase homogeneity. It can be noted that **1** is formed as rod-like crystals with numerous leaves. In contrast to **1**, the surface morphology of **2** appears as a block with a lot of fractures. Energy-dispersive X-ray spectroscopy (EDS) analysis was also carried out to detect the composition of the as-fabricated compounds, as shown in Fig. S5.† Cu, O, N and C were all detected, which are in agreement with the crystal structure analysis.

3.6 Thermogravimetric analysis

Thermogravimetric analysis (TGA) and differential scanning calorimetry (DSC) for compounds **1** and **2** were carried out in a flowing air atmosphere with a heating rate of 10 °C min^{-1} from room temperature to 900 °C (Fig. S6†). Each of these compounds depicts no mass loss until 180 °C, thus confirming the absence of crystallization water molecules. Thereafter, both of them exhibit two steps of mass loss in the temperature range of ~180–270 °C and ~270–500 °C respectively. The first mass loss of **1**, supported by an endothermic effect, corresponds to the removal of the two 2-amino-3-hydroxypyridine moieties 38% (calc. 40%). The second process, which is also associated with endothermic effect, proceeds with a 32% (calc. 35%) and involves the formation of a CuO residue (Fig. S8a†).

In contrast to the case of **1**, the first mass loss of 78% (calc. 81%) in **2** immediately involves the formation of the CuO residue. It deserves to be noted that during the first stage, an unstable product was formed at 195 °C, which was suddenly decomposed to yield the residue. The formation of this product is associated with the exothermic effect, and that of the residue is with the endothermic effect. After that, **2** shows a little mass loss 2% (calc. 3%), supported by an endothermic effect, which can be due to the release of CO_2 (Fig. S8b†).

To confirm the nature of the residue obtained in each compound, they were characterized by X-ray powder diffraction analysis. The powder XRD patterns for both residues were in agreement with the reported pattern of CuO (Fig. S8†).

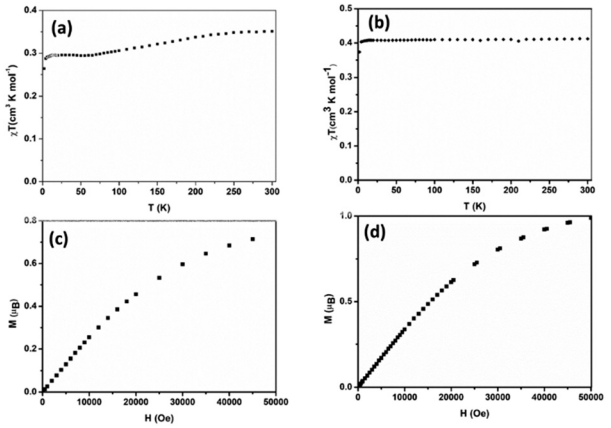

Fig. 6 Temperature dependence of the χT product (top) and field dependence of the magnetization (bottom) of **1** (a and c) and **2** (b and d).

3.7 Magnetic properties

The temperature dependence of the χT product (χ is the magnetic susceptibility) of **1** and **2** is shown in Fig. 6a and b, respectively. The field dependence of the magnetization per formula unit $M_1 = M_{mol}/N_A\mu_B$ at a constant temperature is shown in Fig. 10c and 10d for **1** and **2**, respectively.

For complex **1**, the value of χT at room temperature is 0.36 cm^3 K mol^{-1}, which perfectly matches the calculated value of one isolated Cu^{2+} ion (0.36 cm^3 K mol^{-1}, S = 1/2). Upon cooling, χT decreases slowly down to 65 K where it reaches almost a plateau (0.30 cm^3 K mol^{-1}) down to 10 K. Below this temperature, χT decreases again. The decrease of χT in the high temperature regime together with the plateau could suggest a system involving an odd number of antiferromagnetically coupled spin S = 1/2. However, it was not possible to fit the experimental data with such systems. Furthermore, this is not realistic due to the crystal structure as described above. It shows a network of hydrogen bonds that link the $(C_5H_7N_2O)_2[Cu(C_2O_4)_2]$ entities in the form of a 1D chain but are in no way compatible with an odd spin system. Fitting the experimental by considering a 1D chain of S = 1/2 was also unsuccessful. In any case, in this compound, the intermolecular bonding network consisting mainly of hydrogen bonds, even reinforced by the π–π stacking between the pyridine rings, is not expected to transmit such strong magnetic exchange interactions.[36] A possible explanation may be a phase transition occurring below 65 K, which is below the reach of our X-ray diffraction setups.

For complex **2**, the value of χT is 0.4 cm^3 K mol^{-1} at room temperature, a value which is close to the value expected for one isolated Cu(II) (0.36 cm^3 K mol^{-1}). Upon cooling, χT remains constant for almost all temperature domain and decreases only below 10 K. This feature indicates that Cu(II) are almost magnetically independent of the occurrence of very weak antiferromagnetic interactions between the Cu(II) centers operating only below 10 K. This is in agreement with axial coordination and the bridge angle (Cu–O–Cu) of 110.81° of the single oxygen-bridged Cu(II) ions within one-dimensional chain. This does not allow any overlap with the $d_{x^2-y^2}$ magnetic orbital and does not promote any strong magnetic exchange interaction between the Cu(II) centers.[37] It has also been demonstrated by Oshio and Nagashima[38] through theoretical calculations on 1D chains of copper(II) complexes using the Heisenberg linear chain model, showing that the weak antiferromagnetic interaction in the chain is due to the long axial Cu–O bond length (*ca.* 2.54 Å), which causes a small induction of the spin on the d_{z^2} orbital of the nearby complex. Therefore, the weak antiferromagnetism observed is in agreement with the value of the axial Cu–O bond length, 2.454(2) Å, in this compound.

In order to confirm the magnetic coupling observed in **1** and **2**, the magnetic field dependence of the magnetization $M(\mu_B)$ (Fig. 6c and d) has been measured. From the obtained curve, it is well observed that for both compounds, the magnetization M has reached B = 5 T, a saturation plateau. It is important to recall at this stage that it is well known for Cu(II) complexes with ground state S = 1/2 that the magnetization $M(\mu_B)$ should be saturated to the value of M_{sat} = 1.0 μ_B. In the case of **1**, the magnetization (M = 0.73 μ_B at B = 5 T) was saturated below the value expected for one isolated Cu(II) (M_{sat} = 1.0 μ_B) (Fig. 6c). This indicates rather sizable (negative) J-values and may be due to the paramagnetic impurities, which could have an influence on the interaction between the paramagnetic centers.[36] In contrast to what has been observed in **1**, the magnetization in **2** was saturated to the value expected for one isolated Cu(II) (Fig. 6d).

4. Conclusions

We report two pyridinium copper(II) oxalate organic–inorganic salts, namely, $(C_5H_7N_2O)_2[Cu(C_2O_4)_2]$ **1** and $C_{13}H_{16}N_2[Cu(C_2O_4)_2]$ **2**, exhibiting differences in i) the coordination mode of oxalate ligands, ii) the coordination geometry around Cu(II) and iii) the supramolecular association ($C_5H_7N_2O$ = 2-amino-3-hydroxypyridinium; $C_{13}H_{16}N_2$ = 4,4′-trimethylenedipyridinium). One remarkable feature of **2** is that the oxalate(2-) ligand has adopted the unusual μ-oxalato-$\kappa^3O^1,O^2:O^{1\prime}$ coordination mode. Moreover, in **2** $[Cu(C_2O_4)_2]^{2-}$ anions polymerize *via* the axial Cu–O bond, leading to a uniform zigzag Cu(II) chain with a Cu···Cu separation of 5.32 Å, whereas in **1** they do not polymerize. These differences between **1** and **2** reveal that the cationic species play key roles in tuning the architectures of the target compounds. Regarding the thermal stability of these compounds, both were found to be stable up to 180 °C. Magnetic studies reveal the weak antiferromagnetic interactions in compounds **1** and **2**. This work not only expands the family of copper(II) oxalate salts involving pyridinium type counterions, but also further provides insight into the influence of these cations on the crystal architecture. However, existing correlations which could make the structural architecture of such salts controllable are to be discovered yet.

Conflicts of interest

There are no conflicts to declare.

Acknowledgements

CLDF, LÖ and JN are thankful to the Swedish Research Council for funding, and the Berkeley Global Science Institute (BGSI) for a supporting network. AKI acknowledges support from the Swedish Foundation for Strategic Research (SSF). We gratefully acknowledge Mr Erik Svensson Grape (Stockholm University) for the SEM analysis, Mr David Kiefer (Chalmers University of Technology) for the TGA measurements and Chalmers Materials Analysis Laboratory, CMAL, and the Olle Enqvist Foundation for funding the single crystal diffractometer.

Notes and references

1 L. Öhrström and J. Covès, The Rhubarb Connection and Other Revelations: The Everyday World of Metal Ions, https://pubs.rsc.org/en/content/ebook/978-1-78801-094-8, Royal Society of Chemistry, London, 2018.
2 C. L. F. Dazem, F. M. A. Noa, J. Nenwa and L. R. Öhrström, *CrystEngComm*, 2019, **21**, 6156–6164.
3 J. Y. Lee, M. G. Hur, Y. B. Kong, E. J. Lee, S. D. Yang, P. S. Choi and J. H. Park, *J. Radioanal. Nucl. Chem.*, 2021, **330**, 455.
4 H.-M. Li, G.-M. Zhong, S.-Q. Wu, O. Sato, X.-Y. Zheng, Z.-S. Yao and J. Tao, *Inorg. Chem.*, 2021, **60**, 8042–8048.
5 Z.-L. Xie, L. Deng, C. Yuan, W.-Z. Weng and Z.-H. Zhou, *Inorg. Chem. Commun.*, 2021, **129**, 108661.
6 N. Marino, M. L. Calatayud, M. Orts-Arroyo, A. Pascual-Álvarez, N. Moliner, M. Julve, F. Lloret, G. De Munno, R. Ruiz-García and I. Castro, *Magnetochemistry*, 2021, **7**, 65.
7 L. Wang, W. Wang, D. Guo, A. Zhang, Y. Song, Y. Zhang and K. Huang, *CrystEngComm*, 2014, **16**, 5437–5449.
8 Y. Y. Sun, Y. X. Zong, H. R. Ma, A. Zhang, K. Liu, D. B. Wang, W. Q. Wang and L. Wang, *J. Solid State Chem.*, 2016, **237**, 225–233.
9 C. J. Kepert, *Chem. Commun.*, 2006, 695–700, DOI: 10.1039/B515713G.
10 X. Chen, S. Han and R. Wang, *CrystEngComm*, 2012, **14**, 6400–6403.
11 M.-H. Zeng, W.-X. Zhang, X.-Z. Sun and X.-M. Chen, *Angew. Chem., Int. Ed.*, 2005, **44**, 3079–3082.
12 O. Castillo, A. Luque, P. Román, F. Lloret and M. Julve, *Inorg. Chem.*, 2001, **40**, 5526–5535.
13 O. Castillo, A. Luque, F. Lloret and P. Román, *Inorg. Chim. Acta*, 2001, **324**, 141–149.
14 C. F. N. Nguemdzi, F. Capet, J. Ngouné, G. Bebga, M. Foulon and J. Nenwa, *J. Coord. Chem.*, 2018, **71**, 1484–1496.
15 F. A. Cotton, G. Wilkinson, C. A. Murillo and M. Bochmann, *Advanced Inorganic Chemistry*, Wiley, New York, 6th edn, 1999.
16 C. L. F. Dazem, B. N. Ndosiri, E. N. Nfor, R. Köferstein, P. Shankhari, B. P. T. Fokwa and J. Nenwa, *J. Mol. Struct.*, 2020, **1203**, 127399.
17 J. Nenwa, E. D. Djomo, E. N. Nfor, P. L. Djonwouo, M. Mbarki and B. P. T. Fokwa, *Polyhedron*, 2015, **99**, 26–33.
18 I. N. Kamga, B. N. Ndosiri, A. N. Nana, T. Roman, L. S. Pouamo and J. Nenwa, *Polyhedron*, 2021, **205**, 115291.
19 A. Earnshaw, *Introduction to Magnetochemistry*, Academic Press, London, 2nd edn, 1968.
20 M. A. Viswamitra, *J. Chem. Phys.*, 1962, **37**, 1408–1414.
21 G. Sheldrick, *Acta Crystallogr., Sect. A: Found. Adv.*, 2015, **71**, 3–8.
22 O. V. Dolomanov, L. J. Bourhis, R. J. Gildea, J. A. K. Howard and H. Puschmann, *J. Appl. Crystallogr.*, 2009, **42**, 339–341.
23 P. A. Gaye, A. D. Sarr, M. Gaye, M. Sanselme and P. V. Agasse, *Acta Crystallogr., Sect. E: Struct. Rep. Online*, 2011, **67**, m1046.
24 Z.-C. Pan, K.-L. Zhang and S. W. Ng, *Acta Crystallogr., Sect. E: Struct. Rep. Online*, 2008, **64**, m221.
25 Y.-Q. Sun, J. Zhang, J.-L. Chen and G.-Y. Yang, *Eur. J. Inorg. Chem.*, 2004, **2004**, 3837–3841.
26 R. Selvakumar, S. J. Geib, T. Premkumar and S. Govindarajan, *J. Therm. Anal. Calorim.*, 2016, **124**, 375–385.
27 K. Matelková, L. Kucková, A. Mašlejová, J. Moncoľ, V. Jorík and J. Kožíšek, *Chem. Pap.*, 2016, **70**, 82–92.
28 F. Klongdee, J. Boonmak and S. Youngme, *Acta Crystallogr., Sect. C: Struct. Chem.*, 2018, **74**, 300–306.
29 W. Li, H.-P. Jia, Z.-F. Ju and J. Zhang, *Inorg. Chem. Commun.*, 2008, **11**, 591–594.
30 K. Muraleedharan and S. Kripa, *J. Anal. Appl. Pyrolysis*, 2014, **107**, 298–305.
31 Y.-H. Xiao, Z.-P. Deng, Z.-B. Zhu, L.-H. Huo and S. Gao, *Dalton Trans.*, 2017, **46**, 16493–16504.
32 N. K. Singh, M. K. Bharty, R. Dulare and R. J. Butcher, *Polyhedron*, 2009, **28**, 2443–2449.
33 W. E. Hatfield and T. S. Piper, *Inorg. Chem.*, 1964, **3**, 841–843.
34 M. Zhou, L. Song, F. Niu, K. Shu and W. Chai, *Acta Crystallogr., Sect. C: Cryst. Struct. Commun.*, 2013, **69**, 463–466.
35 S. Roy, P. Mitra and A. K. Patra, *Inorg. Chim. Acta*, 2011, **370**, 247–253.
36 M. Barwiolek, E. Szlyk, A. Kozakiewicz, T. Muziol, A. Bieńko and J. Jezierska, *Dalton Trans.*, 2018, **47**, 13902–13912.
37 D. J. Hodgson, in *Prog. Inorg. Chem.*, 1975, ch. 4, pp. 173–241, DOI: 10.1002/9780470166208.
38 H. Oshio and U. Nagashima, *Inorg. Chem.*, 1992, **31**, 3295–3301.